This research was published in the FASEB Journal. Roy, S., Boiteux, C., Alijevic, O., Liang, C., Berneche, S., and Kellenberger, S. (2013) Molecular determinants of desensitization in an ENaC/degenerin channel. FASEB J 27, 5034-5045, doi: 10.1096/fj.13-230680

Molecular determinants of desensitization in an ENaC/degenerin channel

Sophie Roy[1], Céline Boiteux[2], Chungwen Liang[2], Simon Bernèche[2] and Stephan Kellenberger[1]

[1]Department of Pharmacology and Toxicology, University of Lausanne, Bugnon 27, CH-1005 Lausanne, Switzerland

[2]Swiss Institute of Bioinformatics, Biozentrum, University of Basel, CH-4056 Basel, Switzerland

Running title: Role of the ASIC palm domain in desensitization

Correspondence to:

Stephan Kellenberger
Department of Pharmacology and Toxicology
University of Lausanne
Rue du Bugnon 27
CH-1005 Lausanne
Switzerland
Phone ++4121 692 5422
Fax ++4121 692 5355
Stephan.Kellenberger@unil.ch

Abbreviations

ASIC, acid-sensing ion channel; DMBE-MTS, methanesulfonothioic acid 3,3-dimethylbutyl ester; ENaC, epithelial Na^+ channel; I_{peak}, peak current; I_{sust}, sustained current; MTS, methane thiosulfonate; MTSES, 2-sulfonatoethyl methanethiosulfonate ; MTSET, 2-trimethylammonium-ethyl methanethiosulfonate ; MD, molecular dynamics; WT, wild type.

Abstract

Epithelial Na^+ channel (ENaC)/degenerin family members are involved in mechanosensation, blood pressure control, pain sensation and the expression of fear. Several of these channel types display a form of desensitization, allowing the channel to limit Na^+ influx during a prolonged stimulation. We used site-directed mutagenesis and chemical modification, functional analysis and molecular dynamics simulations to investigate the role of the lower palm domain of the acid-sensing ion channel 1, a member of the ENaC/degenerin family. The lower palm domains of this trimeric channel are arranged around a central vestibule, at ~20 Å above the plasma membrane. They are covalently linked to the transmembrane channel parts. We show that the lower palm domains approach each other during desensitization. Residues in the palm domain co-determine the pH dependence of desensitization, its kinetics, and the stability of the desensitized state. Mutations of palm residues impair desensitization by preventing the closing movement of the palm. We identify and describe here the function of an important regulatory domain that likely has a conserved role in ENaC/degenerin channels.

Key Words: ASIC, channel gating, molecular dynamics, pH

Introduction

The Epithelial Na^+ channel (ENaC)/degenerin family of ion channels comprises among others the degenerins involved in touch sensation, ENaC that plays an important role in Na^+ balance and blood pressure control, and the acid-sensing ion channels (ASICs) whose functions include pain sensation, the expression of fear and neurodegeneration after ischemic stroke (1-3). ENaC/degenerin proteins form Na^+-selective channels that share a common subunit organization (4). Functional ASICs are formed by homo- or heterotrimeric assembly of ASIC subunits 1a, 1b, 2a, 2b and 3. Each subunit consists of a large extracellular domain, two transmembrane helices and short cytoplasmic N- and C-termini. Crystal structures of the transmembrane and extracellular parts of chicken ASIC1 indicated a hand-like shape of the single subunits that are arranged back to back around the central vertical channel axis (5-8). Accordingly, different domains have been named as finger, thumb, knuckle, β-ball and palm, as illustrated in Fig. 1A. Extracellular acidification opens ASICs rapidly but only transiently. Within hundreds of milliseconds the channels enter the non-conducting desensitized state in the continued presence of the acidic pH. Desensitization protects ASIC-expressing cells from excessive loading with Na^+ during prolonged stimulation.

The mechanisms of ENaC/degenerin channel gating are currently only incompletely understood. Several studies concluded that protonation of several residues per subunit in the extracellular domains finger, thumb and palm is required for ASIC activation (7, 9, 10), which involves the opening of the gate located in the transmembrane domain (5, 11). The palm domain, forming a β strand-rich scaffold along the vertical axis of the protein, is the covalent link between the extracellular and transmembrane domains. In addition, the "β-turn" located in a loop between the thumb and the palm, makes hydrophobic interactions with residues of the outer end of the first transmembrane segment and is critical for relaying protonation of extracellular residues to pore opening (12). Functional studies with mutations of the palm residue ASIC1a-E418 had suggested that the conformation of the lower palm region may change during desensitization (10).

In this study we examine the role of the lower palm of ASIC1a and its conformational changes during channel activity. By combining site-directed mutagenesis and chemical modification with functional analysis and molecular dynamics (MD) simulations we show that the lower palm is critically involved in desensitization and we provide evidence that it undergoes a closing movement during desensitization. Substitutions of palm residues affect both the time course of desensitization as well as the stability of the desensitized state.

Mutations in the palm that impair desensitization do so by preventing the conformational changes of the lower palm.

Materials and Methods

Site-directed mutagenesis and expression in Xenopus oocytes

The original human ASIC1a cDNA construct was kindly provided by D. Corey (13). Mutations were introduced by Quikchange (Agilent, Basel, Switzerland) and verified by sequencing (Synergene Biotech, Zurich, Switzerland). Expression in *Xenopus* laevis oocytes was carried out as described previously (14). Complementary RNAs were synthesized *in vitro*. Oocytes were surgically removed from the ovarian tissue of female *Xenopus laevis* which had been anaesthetized by immersion in 2 g l^{-1} MS-222 (Sandoz, Basel, Switzerland). All experimental procedures on *Xenopus laevis* were realized according to the Swiss federal law on animal welfare, approved by the committee on animal experimentation. Healthy, defolliculated stage V and VI *Xenopus* oocytes were isolated and pressure-injected with 50 nl of cRNA solution and oocytes were kept in modified Barth solution during the expression phase.

Electrophysiological analysis

Electrophysiological measurements were carried out 18 - 48 h after cRNA injection as described previously (14). Macroscopic currents were recorded using two-electrode voltage-clamp at –60 mV with a Dagan TEV-200 amplifier (Minneapolis, MN, USA), and analyzed with the pCLAMP data acquisition package (Molecular Devices, Silicon Valley, CA). The standard bath solution contained 110 mM NaCl, 2.0 mM $CaCl_2$, 10 mM Hepes-NaOH, (or MES-NaOH for pH<6.8), and pH was adjusted by NaOH to the values indicated. Oocytes were perfused by gravity at a rate of 5-15 ml/min. The pH activation curves were fitted to the Hill equation: $I = I_{max}/[1+(10^{-pH50}/10^{-pH})^{nH}]$, where I_{max} is the maximal current, pH50 is the pH of half-maximal current amplitude and n_H is the Hill coefficient, using KaleidaGraph (Synergy software, Reading, PA, USA). Steady-state desensitization curves were fitted by an analogous equation. Current kinetics were fitted by a single exponential. Outside-out patches were obtained and measured as described previously (14). Solutions were changed with an ultra-rapid piezo-driven system (MXPZT-300L, Siskiyou, Grants Pass, OR, USA). Data are presented as mean ± SEM. Differences between hASIC1a WT and mutants were analyzed by ANOVA followed by Dunnet post hoc test ($p < 0.05$). In experiments with methane thiosulfonate (MTS) reagents, functional parameters were measured before and after a 5-min

incubation with the reagent. In these experiments the paired student t-test was used to determine significance of the effect of MTS reagents.

Molecular dynamics simulations

The atomistic models were built using the charmm-gui web service based on the x-ray structure of WT chicken ASIC1 (PDB code: 2QTS) (7). The channel was embedded in a bilayer composed of 348 DPPC lipid molecules and solvated with ~43,000 water molecules. Counter-ions (Na^+ and Cl^-) were added to neutralize the system and mimic a salt-concentration of ~150 mM. The system contains a total of ~197,000 atoms. Based on Poisson-Boltzmann pKa calculations, the following residues had a pKa >7 and were thus protonated: E63, D78, E79, E97, E177, E238, E242, E277, E315, D351, D409, D434 (numbering of human ASIC1a) (10). Mutant systems (L77R, Q276R, L280R, L415R, and N416R) were constructed with the same procedure. In the simulation of the L280R mutant, residue E79 interacts directly with R280 and was thus not protonated.

All-atom MD simulations were performed using the NAMD 2.9b2 package (15) with the CHARMM force field (16) for proteins (v27) and lipids (v36), and the TIP3P model for the water molecules. During all simulations, the SETTLE algorithm was used to constrain bond lengths and angles of water molecules, and the LINCS algorithm was used for all other bonds and angles involving hydrogen atoms, allowing an integration time step of 2 fs. Long-range electrostatic interactions were calculated using the Particle-Mesh-Ewald (PME) method (17) and short-range repulsive and attractive dispersion interactions were described with Lennard-Jones potentials, using a cutoff length of 1.2 nm. The temperature of the system was kept constant using Langevin dynamics with an external heat bath at 323 K. Similarly, the pressure along the membrane normal (z direction) was kept constant to 1 bar. The simulation time was 32 ns for WT, 24 ns for L77R, 20 ns for Q276R, 38 ns for L280R, 34 ns for L415R and 28 ns for N416R. Note that the stochastic behavior of the simulations leads to asymmetries that reflect the conformational space accessible to the protein. On longer simulation time-scale all subunits should visit the same states, but not necessarily at the same time. Molecular graphics were prepared using the UCSF Chimera package (18).

Reagents

The MTS reagents DMBE-MTS (methanesulfonothioic acid 3,3-dimethylbutyl ester), MTSES (2-sulfonatoethyl methanethiosulfonate) and MTSET (2-trimethylammonium-ethyl methanethiosulfonate) were obtained from Toronto Research Chemicals (Montreal, Canada),

and other reagents were from Sigma, Fluka (Buchs, Switzerland) or Applichem (Darmstadt, Germany).

Results

Palm residues pointing towards the central cavity show a low solvent accessibility in closed channels

The lower palm domain is made up of a β sheet in each subunit. The β sheets of the three subunits are arranged around the central cavity located at ~20 Å above the extracellular end of the transmembrane domain, forming a funnel-like structure (Fig. 1A). Each β sheet is composed of four β strands with two of them (β9 and β10) stretching the entire length of the palm. β1 and β12 are shorter and are connected by the β1– β2 and β11- β12 linkers to β strands located higher up in the β-ball and the palm, respectively. The side chains of the lower palm β sheets point alternatingly towards the central cavity or towards the outside of the lower palm (Fig. 1A).

To measure the solvent exposure of lower palm residues, they were mutated individually to Cys and the mutant channels were exposed to the sulfhydryl reagent MTSET that adds a positively charged group to Cys residues. Extracellular application of this reagent does not affect the function of wild type (WT) ASIC1a (10). For many mutants the modification by MTSET changed channel function, allowing measurement of the kinetics of sulfhydryl modification, as illustrated for L280C (Fig. 1B). Exposure of L280C channels to MTSET resulted in the appearance of a sustained current and a moderate increase of the peak current amplitude. An exponential fit of the time course of the appearance of the sustained current fraction yielded the rate of modification of residue C280 by MTSET (Fig. 1C). Similarly, MTSET induced various functional changes in other lower palm Cys mutants (Supplemental Table S1) allowing the calculation of the rate of modification by MTSET. The MTSET modification rate of closed channels differed importantly between residues (Fig. 1D). Fig. 1E shows the lower palm region in the structural model of ASIC1a (10) with the palm residues of one subunit colored according to the MTSET reaction rate on their Cys substitution mutants. The highest reaction rates were measured for residues pointing outwards, most of them located in the lower part of the β sheet (green and orange), followed by outwardly pointing residues of the upper part of β strand 12 and the β11- β12 linker (pink). The residues pointing into the central cavity showed all lower reaction rates, consistent with the lower solvent accessibility predicted from the crystal structure.

The lower palm domain closes during desensitization

If the lower palm β sheets move towards each other during desensitization, the inwardly pointing residues should be less accessible and therefore their modification rate should be lower in the desensitized than in the closed state. To compare the accessibility of palm residues in the closed and desensitized states we applied MTSET to channels that were in either of these functional states. We lowered the extracellular Ca^{2+} concentration without changing the pH to switch from the closed to the desensitized state (19, 20). By keeping the pH constant we avoided possible artifacts due to the intrinsic pH dependence of the sulfhydryl reaction, unrelated to channel function. Fig. 2A shows the steady-state desensitization (SSDES) curve of the mutant E418C measured either in the presence of 0.1 mM or 2 mM Ca^{2+}. The SSDES curve plots the fraction of available channels as a function of the conditioning pH and shows that at pH7.6 the E418C channels were almost completely desensitized in 0.1 mM Ca^{2+}, but that no desensitization had occurred in 2 mM Ca^{2+} at this pH. Oocytes expressing E418C were exposed during 2 min at pH7.6 to an MTSET concentration estimated to modify 60-80% of the closed channels, in the presence of either 2 mM (closed channels) or 0.1 mM Ca^{2+} (desensitized channels, Fig. 2B). After this 2-min exposure and subsequent current measurement, the closed channels were exposed during 3 min to 1 mM MTSET (pH7.6, 2 mM Ca^{2+}), resulting in 100% modification, and their function was again measured. MTSET at 0.16 mM readily modified E418C when applied to closed channels (upper middle trace, 2 mM Ca^{2+}), but not when applied to desensitized channels (lower middle trace, 0.1 mM Ca^{2+}, Fig. 2B). The fractional modification of E418C and other lower palm mutants is plotted for closed and desensitized channels in Fig. 2C. The fractional modification by MTSET was reduced by desensitization in all residues tested that point towards the central cavity (blue in Fig. 2D). The modification of some of the outwardly pointing residues was state-independent (orange). The D78C and to a stronger extent the Y417C mutant – both pointing outwards - were more rapidly modified in the desensitized state, suggesting that these residues (green) are less exposed in the closed state than they appear in the desensitized crystal structure. These observations strongly suggest that the lower palm undergoes a closing movement during desensitization.

The movement of the lower palm determines the desensitization kinetics

We observed that substitution of almost any of the lower palm residues affected the pH dependence of steady-state desensitization, the direct transition from the closed to the desensitized state at pH slightly below physiological values (Supplemental Table S2). This

illustrates the central role of the lower palm in desensitization. The pH dependence of activation was affected to a lesser extent (Supplemental Table S2). To examine the desensitization from open channels we measured the kinetics of the decay phase of the macroscopic currents. The V414C mutant desensitized with slower kinetics than the WT, and desensitization was further slowed after MTSET modification (Figure 3A). Similarly, the N416C mutant displayed slowed desensitization kinetics after MTSET exposure. The time constants of desensitization obtained from single exponential fits to the decaying phase of the current are plotted in Figure 3B for different other mutants. Modification of residues in the β11-β12 linker, as well as a "belt" of residues in the center of β9, β10 and β12 affected open-channel desensitization (Figure 3C). Substitution of two outward facing residues accelerated desensitization. For most residues the substitution by Cys still allowed normal desensitization kinetics and a slowing or acceleration was only observed after MTSET modification (* in Figure 3C).

Under a stimulation of pH≤6 the open-channel desensitization kinetics of WT ASIC1a and most mutants were pH-independent (Fig. 3D). Interestingly, a pH dependence was uncovered in some mutants, with a striking acceleration of open-channel desensitization at more acidic pH for N416C-MTSET and Q278C-MTSET, and a slowing at acidic pH for Q278C (Fig. 3D). The residue N416 is located at the upper end of β strand 12. In the desensitized structure its side chain points outward and forms hydrogen bonds with the β1-β2 linker (Fig. 3E-F), which is critical for the kinetics of open-channel desensitization (21). In the recently published Psalmotoxin-bound open ASIC1 structure the upper end of β12 is twisted, suggesting that N416 undergoes a substantial change in side chain orientation during the open-desensitized transition (Fig. 3E (5)). We carried out MD simulations based on the desensitized structure with the N416R mutant, which is chemically similar to the MTSET-modified N416C. In the adopted desensitized conformation the R416 side chain points diagonally outward, oriented towards β9 and making hydrogen bonds with the β1- β2 linker and with side chains of other palm residues such as E413 and E277 (Fig. 3G). This orientation towards β9 in the mutant as opposed to the orientation towards the side of β1 in WT is likely due to sterical constraints and to hydrogen bond formation with other palm residues. Moving from the orientation adopted in the open channel to that of the desensitized state requires a larger movement in the mutant, which in addition will be harder for this bulky and charged side chain, potentially explaining the observed slowing of desensitization. The observed acceleration of

desensitization of N416C-MTSET channels under acidic pH might be due to protonation of an acidic side chain interacting with residue 416 in the open conformation.
Alternatively, the slowing of the current decay phase observed in several mutants might reflect slowing of channel opening. However, the opening time constant at pH5 of MTSET-modified V414C and N416C, measured from outside-out patches was not different from that of WT (5.2 ± 1.5 and 4.4 ± 1.6 ms, respectively, compared to 4.1 ± 1.0 ms, n=3), excluding this possibility.

Substitution of distinct lower palm residues impairs desensitization
Wild type hASIC1a currents desensitize completely during the acidic stimulation, resulting in a sustained/peak current ratio (I_{sust}/I_{peak}) of < 0.01 (Fig. 3A). For some residues in the lower palm domain, substitution resulted in the appearance of a non-desensitizing (sustained) current (Fig. 4A-B). In these channels the desensitized state is less stable than in WT, and channels can switch between the open and the desensitized state during the acidic stimulation leading to the observed I_{sust}. Substitution of the residues Q276 and Q278 of β9, L415 of the β11-β12 linker, and a belt of hydrophobic residues of the β sheet pointing towards the central vestibule (L77, I420, L280) destabilized the desensitized state (Fig. 4C). L415C showed a small, rapidly desensitizing peak, followed by a slowly developing sustained current (Fig. 4A, upper right panel). After exposure to MTSET the initial transient peak disappeared and the activation kinetics of the sustained current were accelerated.
To determine for five selected residues the properties of the side chains that were important for desensitization, Cys mutants were exposed to the negatively charged MTSES or the non-polar DMBE-MTS, and in addition mutations to Arg were made. I420 appeared to be able to accommodate many different types of side chains without a change in I_{sust}, except for the positively charged MTSET (Fig. 4D). Mutation to Arg, which was made to mimic the Cys-MTSET side chain although being smaller, induced in all mutants an I_{sust}. The I_{sust} fraction of Arg mutants was however in most mutants smaller than in the Cys-MTSET substitution. For L77, Q276, L280 and L415 the size of the engineered side chain was as important as its charge, since modification by MTSET and DMBE-MTS gave similar I_{sust} fractions (Fig. 4D).

Mutations impair desensitization by changing the conformation of the lower palm domain
To determine the structural changes underlying the increased I_{sust} we carried out MD simulations with ASIC1 WT and with the mutants L77R, Q276R, L280R and L415R. L415,

located in the β11-β12 linker, and L77, Q276 and L280 of the lower palm β sheet are all oriented towards the central cavity. Comparison of the crystal ASIC1 structures shows that at the level of the upper half of the lower palm β sheets the central vestibule is wider in the open than in the desensitized channel (5). The conformation of the individual β sheets is however conserved in the open channel structure, except for an opening between the upper parts of β12 and β9 (Supplemental Fig. S1A). This suggests that in the open-to-desensitized transition the β sheets mostly move as a whole. In MD simulations we observed small differences to WT in the β sheet hydrogen bond pattern in L77R and L280R (Supplemental Fig. S1B). The L415R mutation produced in one subunit a marked separation of the upper parts of β1, β12 and β9.

Figure 5A plots the radius of the cavities along the central vertical axis of the channel (22). In the open structure the central cavity is widest at the level of R371 and Q276 (Fig. 5B). At the lower end of the central cavity, at the level of L77, a narrow constriction is formed. In MD simulations, the radius of the central cavity was smaller in the desensitized conformation of the WT than in the open crystal structure, and the constriction was less pronounced (Fig. 5A). Such a difference in the radius of the central cavity had previously been described between the desensitized and the open crystal structure (5). The L280R mutant showed in MD simulations a wider central cavity than the WT. This widening occurred at a lower level and over a longer part of the palm than that seen in the open channel structure (Fig. 5A). The two mutants L77R and Q276R displayed a constriction similar to that of the open structure. Q276R led in addition to a narrowing of the central cavity. Q276 and L280 are located close to the edges of the β sheets and point towards neighboring β sheets, as illustrated in a schematic view from the bottom of the palm (Fig. 5C). L77 in contrast points towards the center. A side view of the palm illustrates that L77 sits at the bottom of the central cavity, contributing to the observed constriction, and L280 as well as Q276 are located higher up (Fig. 5D, view from inside of the palm). The “opening” of the palm induced by the L280R mutation is illustrated by the aligned structures of WT and the L280R mutant in side view and from the bottom (Fig. 5E-F). In the MD simulation this conformational change was asymmetrical, moving mostly the subunit A outwardly (Fig. 5F, Supplemental Figs. S1C-D & S2). Inspection of the palm conformation at the end of the MD simulations showed that in the three mutants the acidic residues E79 and E418 were important for accommodating the introduced basic side chain. The L280R side chains were arranged horizontally, pointing towards the two Glu residues of a neighboring subunit and thereby pushing the palm open

(Fig. 5G). A basic side chain on the same subunit, R371, prevented R280 from folding upwards. The R77 side chains were oriented vertically, interacting with Glu residues of the same subunit (mostly E418, Fig. 5H). This placement of the side chains led to a narrowing of the lower part of the central vestibule. The Q276 side chain was in the WT in close proximity of the Glu residues of the same subunit, and of R371 of a neighboring subunit (Fig. 5D). The engineered Arg at position 276 formed a salt-bridge with the Glu residues of the same subunit, pointing more downward than in the WT (Fig. 5I). As a result of the competition of R276 interacting with E79, and of the electrostatic repulsion, the neighboring R371 pointed upward, toward E413. This led to the narrowing of the constriction and of the upper half of the central vestibule, as documented in Fig. 5A and confirmed by contact maps and distance measurements at the level of L74 and E418 (Supplemental Figs. S1C-D & S2).

Structural changes induced by the L415R mutation

L415 is positioned on the β11-β12 linker, next to N416 that co-determines the kinetics of desensitization (Fig. 3). Its side chain orientation changes by almost 180° between the open and the desensitized state ((5), Fig. 6A). L415 is located close to a subunit interface and makes hydrophobic interactions with residues of the β9 and β10 strands of the neighboring subunits and to a smaller extent with the β11- β12 and β1- β2 linker of the same subunit (Fig. 6B). In the simulation of the L415R mutant, in two out of three subunits, the R415 side chain pointed towards the neighboring subunit where it interacted with E254 of the β-ball (Fig. 6C). The R371 residue of the neighboring subunit pointed downward, coming close to E418 and N416, and not to E413 as in the WT. In the third subunit the R415 side chain pointed not to the neighboring subunit, but downwards, pushing the own β1 strand down and outward (Fig. 6D). This disrupted the upper part of the β sheet backbone and is reminiscent of the structural change in the open channel structure (Fig. 6A and Supplemental Fig. S1B). To obtain information on the importance of the interaction of R415 with the neighboring E254 and on the required side chain properties of residue 415 we have functionally analyzed the L415R-E254Q double mutant and several single mutants of L415. Mutation of E254 to Gln in the background of the L415R mutant produced a channel in which the sustained current was retained, indicating that the electrostatic interaction between E254 and R415 is not necessary for the presence of the sustained current (Fig. 6E). Substitution of L415 by the small residues Ala, Cys or Ser resulted in a 100% I_{sust} fraction that became smaller below a certain stimulation pH (Fig. 6E). This decrease in I_{sust} occurred at more acidic pH than in L415R or

L415C-MTSET. Interestingly the pH dependence of activation was similarly shifted to acidic values when L415 was substituted by small residues, but not if the substituting side chain was large, hydrophilic and positively charged as Arg or Cys-MTSET (Fig. 6F). Thus, a positive charge at position 415 could partially prevent the acidic shift in the pH dependence of activation, and of the I_{sust} decrease. The double mutant R371C L415R was non-functional but was transformed into a H^+-gated channel after exposure to MTSET ($I_{pH4.5}$ = 0.1 ± 0 μA before and I_{pH5} = 15.5 ± 5.5 μA after MTSET exposure, n=3-5), indicating that the electrostatic repulsion between R415 and R371 of a neighboring subunit is important for the function and pH dependence of the L415R mutant.

Discussion

We show in this study that the lower palm domains of ASIC subunits move toward the central vertical axis during desensitization. The lower palm domain is critically involved in desensitization, as illustrated by our observations that mutations in this domain affect the time course and the extent of desensitization, as well as the pH dependence of steady-state desensitization. MD analyses show that mutations disrupt desensitization by preventing the lower palm domain from adopting the same conformation as the desensitized WT channel.

Conformational changes in the lower palm during desensitization

The MTSET modification rate of engineered Cys residues in the palm measured on closed channels was substantially smaller for residues oriented towards the central vestibule than for those pointing outward in the crystal structure of the desensitized channel. This indicates that the side chain orientation in the lower palm domain around the central vestibule is similar in the closed and the desensitized state. For residues pointing to the central vestibule the MTSET reaction rate decreased further when the reagent was applied to desensitized channels, indicating that in the desensitized conformation some of them were barely accessible. This strongly suggests that the lower palm domains of the three subunits move towards each other during the transitions from the closed to the desensitized state. Together with the MTSET modification experiments on closed channels it also indicates that the residues do not switch between inward and outward orientation during desensitization. There is evidence that, on the level of E418 in the wide part of the central vestibule, an important part of the closing movement occurs during the transition from the open to the desensitized state. First, intersubunit distances at the level of E79 and E418 were longer in the open than in the desensitized crystal structure (5). Second, mutations of E418 strongly affected desensitization

by sterical hindrance. Activation was however much less affected, indicating that in open channels the palm domains are not as close to each other as they are shown in the desensitized crystal structure (10). A decreased accessibility of E79 after desensitization has also been shown in ASIC3 (20).

Palm sub-domains involved in the open-desensitized transition

Substitution of residues in the β11-β12 linker and of a horizontal belt of residues in the β sheets affected the time course of open-channel desensitization. The residues of the β sheets involved in the desensitization time course only slowed the transition when the engineered Cys residue were modified by MTSET, suggesting that the slowing of desensitization was due to a steric hindrance and/or to electrostatic interactions in the central vestibule.

Three residues in the β1-β2 linker are critical for the desensitization time course in ASIC1 (21). Recent studies have also shown that the β1-β2 and β11-β12 linkers interact with each other (23-25). Comparison of the desensitized and open structures of ASIC1 indicated a twist in the β11-β12 linker leading to a swap of the positions of the side chains L415 and N416 (5). These studies highlighted the importance of these two linkers for channel desensitization, and their requirement of free movement for proper function. In our study, substitutions of N416 slowed desensitization, which was however complete at the end of the acidic stimulation. In MD simulations the N416R mutant adopted a conformation of the R416 side chain that required a larger conformational change for desensitization to occur than in the WT. The charge and the increased size of the mutant side chain likely slowed this movement further down, limiting the kinetics of desensitization.

Effects of desensitization mutations on palm conformation

The appearance of a sustained current after substitution of palm residues supports the important role of the palm domain in desensitization. In these mutants the increased hydrophilicity and size of the side chain caused the disruption of normal desensitization. MD simulations based on the desensitized structure showed that mutations that disrupted desensitization moved the palm away from the WT conformation. The L280R mutation prevented the closure of the palm and was in this respect reminiscent of the open WT structure. Mutation of L77 led to a narrowing of the lower part of the central vestibule. The Q276R mutation led to a narrowing of the upper half of the central cavity and created

additional intersubunit interactions and with it a tighter conformation of the β sheets around the central cavity.

The constriction below the central cavity is seen in both the open and desensitized structures. The three subunits come in contact with each other at the level of residue L77; this is the only contact point along the symmetry axis in the palm domain. Residue L77 may serve as a pivotal point or fulcrum, through which the movements of the palm domain are transmitted to the pore. The outward movement of the palm domains would result, through a rotation around residues L77, into the outward movement of the pore domain helices without the need of creating a cavity throughout the palm domain. Mutation L280R appears to disrupt the contact point formed by residues L77, which are more distant from each other in this mutant. This movement is transmitted to the upper part of the pore domain, which becomes as wide as in the open structure (Fig. 5A), potentially explaining the observed sustained current for the L280R mutant.

In one out of three subunits of the L415R mutant, the introduced Arg in the β11-β12 linker pointed downward, separating the upper parts of the β sheet and pushing β1 downward. Substitutions of L415 behaved differently from substitutions in the β sheet. First, channel function was extremely sensitive to changes of the L415 side chain. Second, substitutions of L415 strongly shifted the pH dependence of activation to more acidic values. This shift was abolished if substitutions were positively charged. Third, most substitutions of L415 disrupted desensitization only completely above a pH threshold. At more acidic pH the I_{sust} decreased, indicating that a sufficiently acidic pH allowed normal desensitization. The pH dependence of activation and of the disappearance of the I_{sust} was in these substitutions highly correlated with the presence of a positive charge at position 415. The presence of R371 was required for the function of the L415R mutant, indicating that the disrupting effect of the substitution is reduced by electrostatic interactions between R415 and R371. Together this suggests that L415 mutations disrupt desensitization by a mechanism that is profoundly different from that of substitutions of β sheet residues, which activated normally but displayed impaired desensitization. The effects of L415 mutations are closer linked to activation and may induce a different type of opening, as has been demonstrated for mutations of the degenerin site, a regulatory site in the ASIC pore (26).

Desensitization as a conserved feature in ENaC/degenerin channels

Other ENaC/degenerin channels than ASICs have been shown to desensitize or to display a transition similar to desensitization. ENaC is regulated by Na^+ self-inhibition in a similar way as protons induce desensitization in ASICs (27, 28). The degenerin current induced by a constant mechanical force is transient (1). FMRFamide-gated Na^+ channels which are members of the ENaC/degenerin channel family also display a desensitizing current (29). The palm is together with the β-ball the most highly conserved domain between ASICs and ENaC (30). Together this suggests that the palm may have a conserved role in desensitization or desensitization-like mechanisms in ENaC/degenerin channels.

Conclusion

The palm domain is involved in linking the pH sensors to the ASIC channel gate. We show here that the lower palm controls desensitization. Upon extracellular acidification the lower palm β sheets undergo a closing movement that stabilizes the desensitized state. For complete and stable desensitization, the lower palm domains must be able to complete the closing movement. The knowledge of the mechanisms of desensitization and the identification of the residues involved in ASIC are valuable for the understanding of ENaC/degenerin channels and for the development of drugs targeting these channels.

References

1. O'Hagan, R., Chalfie, M., and Goodman, M. B. (2005) The MEC-4 DEG/ENaC channel of Caenorhabditis elegans touch receptor neurons transduces mechanical signals. *Nature Neurosci.* **8**, 43-50
2. Schild, L. (2010) The epithelial sodium channel and the control of sodium balance. *Biochim. Biophys. Acta* **11802**, 1159-1165
3. Wemmie, J. A., Price, M. P., and Welsh, M. J. (2006) Acid-sensing ion channels: advances, questions and therapeutic opportunities. *Trends Neurosci.* **29**, 578-586
4. Eastwood, A. L., and Goodman, M. B. (2012) Insight into DEG/ENaC channel gating from genetics and structure. *Physiology* **27**, 282-290
5. Baconguis, I., and Gouaux, E. (2012) Structural plasticity and dynamic selectivity of acid-sensing ion channel-spider toxin complexes. *Nature* **489**, 400-405
6. Gonzales, E. B., Kawate, T., and Gouaux, E. (2009) Pore architecture and ion sites in acid-sensing ion channels and P2X receptors. *Nature* **460**, 599-604

7. Jasti, J., Furukawa, H., Gonzales, E. B., and Gouaux, E. (2007) Structure of acid-sensing ion channel 1 at 1.9 A resolution and low pH. *Nature* **449**, 316-323
8. Dawson, R. J., Benz, J., Stohler, P., Tetaz, T., Joseph, C., Huber, S., Schmid, G., Hugin, D., Pflimlin, P., Trube, G., Rudolph, M. G., Hennig, M., and Ruf, A. (2012) Structure of the Acid-sensing ion channel 1 in complex with the gating modifier Psalmotoxin 1. *Nature commun.* **3**, 936
9. Paukert, M., Chen, X., Polleichtner, G., Schindelin, H., and Grunder, S. (2008) Candidate amino acids involved in H^+ gating of acid-sensing ion channel 1a. *J. Biol. Chem.* **283**, 572-581
10. Liechti, L. A., Berneche, S., Bargeton, B., Iwaszkiewicz, J., Roy, S., Michielin, O., and Kellenberger, S. (2010) A combined computational and functional approach identifies new residues involved in pH-dependent gating of ASIC1a. *J. Biol. Chem.* **285**, 16315-16329
11. Li, T., Yang, Y., and Canessa, C. M. (2011) Outlines of the pore in open and closed conformations describe the gating mechanism of ASIC1. *Nature commun.* **2**, 399
12. Li, T., Yang, Y., and Canessa, C. M. (2009) Interaction of the aromatics Tyr-72/Trp-288 in the interface of the extracellular and transmembrane domains is essential for proton gating of acid-sensing ion channels. *J. Biol. Chem.* **284**, 4689-4694
13. Garcia-Anoveros, J., Derfler, B., Nevillegolden, J., Hyman, B. T., and Corey, D. P. (1997) BNaC1 and BNaC2 constitute at new family of human neuronal sodium channels related to degenerins and epithelial sodium channels. *Proc. Natl. Acad. Sci. USA* **94**, 1459-1464
14. Bargeton, B., and Kellenberger, S. (2010) The contact region between three domains of the extracellular loop of ASIC1a is critical for channel function. *J. Biol. Chem.* **285**, 13816-13826
15. Phillips, J. C., Braun, R., Wang, W., Gumbart, J., Tajkhorshid, E., Villa, E., Chipot, C., Skeel, R. D., Kale, L., and Schulten, K. (2005) Scalable molecular dynamics with NAMD. *J. Comput. Chem.* **26**, 1781-1802
16. Brooks, B. R., Brooks, C. L., 3rd, Mackerell, A. D., Jr., Nilsson, L., Petrella, R. J., Roux, B., Won, Y., Archontis, G., Bartels, C., Boresch, S., Caflisch, A., Caves, L., Cui, Q., Dinner, A. R., Feig, M., Fischer, S., Gao, J., Hodoscek, M., Im, W., Kuczera, K., Lazaridis, T., Ma, J., Ovchinnikov, V., Paci, E., Pastor, R. W., Post, C. B., Pu, J. Z., Schaefer, M., Tidor, B., Venable, R. M., Woodcock, H. L., Wu, X., Yang, W., York,

D. M., and Karplus, M. (2009) CHARMM: the biomolecular simulation program. *J. Comput. Chem.* **30**, 1545-1614

17. Essmann, U., Perera, L., Berkowitz, M. L., Darden, T., Lee, H., and Pedersen, L. G. (1995) A smooth particle mesh Ewald method. *J. Chem. Phys.* **103**, 8577-8593
18. Pettersen, E. F., Goddard, T. D., Huang, C. C., Couch, G. S., Greenblatt, D. M., Meng, E. C., and Ferrin, T. E. (2004) UCSF Chimera - a visualization system for exploratory research and analysis. *J. Comput. Chem.* **25**, 1605-1612
19. Babini, E., Paukert, M., Geisler, H. S., and Grunder, S. (2002) Alternative splicing and interaction with di- and polyvalent cations control the dynamic range of acid-sensing ion channel 1 (ASIC1). *J. Biol. Chem.* **277**, 41597-41603
20. Cushman, K. A., Marsh-Haffner, J., Adelman, J. P., and McCleskey, E. W. (2007) A conformation change in the extracellular domain that accompanies desensitization of acid-sensing ion channel (ASIC) 3. *J. Gen. Physiol.* **129**, 345-350
21. Coric, T., Zhang, P., Todorovic, N., and Canessa, C. M. (2003) The extracellular domain determines the kinetics of desensitization in acid-sensitive ion channel 1. *J. Biol. Chem.* **278**, 45240-45247
22. Smart, O. S., Neduvelil, J. G., Wang, X., Wallace, B. A., and Sansom, M. S. (1996) HOLE: a program for the analysis of the pore dimensions of ion channel structural models. *J. Mol. Graph.* **14**, 354-360, 376
23. Li, T., Yang, Y., and Canessa, C. M. (2010) Asn415 in the beta11-beta12 linker decreases proton-dependent desensitization of ASIC1. *J. Biol. Chem.* **285**, 31285-31291
24. Li, T., Yang, Y., and Canessa, C. M. (2010) Leu85 in the beta1-beta2 linker of ASIC1 slows activation and decreases the apparent proton affinity by stabilizing a closed conformation. *J. Biol. Chem.* **285**, 22706-22712
25. Springauf, A., Bresenitz, P., and Grunder, S. (2011) The interaction between two extracellular linker regions controls sustained opening of acid-sensing ion channel 1. *J. Biol. Chem.* **286**, 24374-24384
26. Champigny, G., Voilley, N., Waldmann, R., and Lazdunski, M. (1998) Mutations causing neurodegeneration in *Caenorhabditis elegans* drastically alter the pH sensitivity and inactivation of the mammalian H^+-gated Na^+ channel MDEG1. *J. Biol. Chem.* **273**, 15418-15422

27. Sheng, S., Bruns, J. B., and Kleyman, T. R. (2004) Extracellular Histidine Residues Crucial for Na^+ Self-inhibition of Epithelial Na^+ Channels. *J. Biol. Chem.* **279**, 9743-9749
28. Horisberger, J. D., and Chraibi, A. (2004) Epithelial sodium channel: a ligand-gated channel? *Nephron Physiol.* **96**, p37-41
29. Lingueglia, E., Champigny, G., Lazdunski, M., and Barbry, P. (1995) Cloning of the amiloride-sensitive FMRFamide peptide-gated sodium channel. *Nature* **378**, 730-733
30. Kashlan, O. B., Adelman, J. L., Okumura, S., Blobner, B. M., Zuzek, Z., Hughey, R. P., Kleyman, T. R., and Grabe, M. (2011) Constraint-based, homology model of the extracellular domain of the epithelial Na^+ channel alpha subunit reveals a mechanism of channel activation by proteases. *J. Biol. Chem.* **286**, 649-660

Acknowledgements

We thank Maxime Blanchard for the activation time course measurements from excised patches. We thank Laurent Schild, Miguel van Bemmelen, Olivier Staub, Karolina Gwiazda, Omar Aljevic, Gaetano Bonifacio and Claudia Suenaga-Lelli for their comments on a previous version of the manuscript. This work was supported by the Swiss National Science Foundation (grant 310030_135542 to SK and SNF Professorship P3_139205 to SB) and by a grant from the Swiss National Supercomputing Center (CSCS) under project ID s241 to SB.

Figure legends

Fig. 1. Accessibility of lower palm residues to MTSET. A, hASIC1a model, illustrating the different domains in one of the three subunits (left panel). The lower palm domain is shown as a structural representation (middle panel) or as a schematic representation (right panel), with outward-facing residues shown in blue, inward-facing residues (i.e. residues oriented towards the central vestibule) in red. **B**, Measurement of the time course of reaction of MTSET on hASIC1a L280C expressed in *Xenopus* oocytes, voltage-clamped to -60 mV. Once every minute the extracellular solution was changed for 5 s from the conditioning pH solution (7.2) to 5.5 to activate ASICs. 0.4 mM MTSET was included in the pH7.2 solution as indicated by the horizontal bar, and the extent of channel modification is reflected by the increase in sustained current. **C**, The sustained/peak current amplitude fraction I_{sust}/I_{peak} is plotted as a function of time for the experiment shown in panel B. The solid line represents an exponential fit, yielding a rate of modification of 0.65 min^{-1}. For B and C, the time point 0 refers to the

start of MTSET perfusion. **D**, MTSET reaction rates in mM^{-1} min^{-1} for application to the closed state are plotted (n=3-10), see Supplemental Table S1 for conditions. Mutants are indicated in the color of their orientation, red (inward facing), blue (outward), black (others). The bars are colored as indicated in E. **E**, Graphical interpretation of data, showing the residues on one of the three subunits, colored according to the MTSET reaction rate on the Cys mutant.

Fig. 2. State-dependent accessibility of lower palm residues to MTSET. A, Steady-state desensitization (SSDES) curve of the mutant E418C at either 0.1 (○) or 2 mM Ca^{2+} (●) in the conditioning solution. The two vertical arrows illustrate the two conditions at pH7.6 used for the experiment described in B, closed, black upward arrow, and desensitized, grey downward arrow. **B**, Illustration of the MTSET accessibility testing to closed (upper traces, pH7.6, 2 mM Ca^{2+}) or desensitized E418C (lower traces, pH7.6, 0.1 mM Ca^{2+}). **C**, The fractional modification by MTSET applied during 2 min to closed or desensitized channels (as illustrated in B, calculated as modification after 2 min of incubation in test conditions / modification after additional 3 min 1 mM MTSET exposure to closed channels) is plotted (n=3-6), see Supplemental Table S1 for conditions. The fractional modification was different between the closed and desensitized state for all mutants except Y282C and E421C ($p<0.01$, t-test). Mutants are indicated in the color of their orientation, red (inward facing), blue (outward), black (others). The bars are colored as indicated in D. **D**, Graphical interpretation of data, showing the residues colored in blue, orange or green if the reaction rate was higher, equal or lower in the closed as compared to the desensitized state.

Fig. 3. Time course of open-channel desensitization. A, Representative traces of WT, V414C and N416C hASIC1a, obtained before and after MTSET modification. **B**, The time constant of open-channel desensitization was determined from single exponential fits to the decaying phase of the current trace induced by pH5 (n=3-21). *, different from WT ($p<0.05$, ANOVA followed by Dunnett's post test). Mutants are indicated in the color of their orientation, red (inward facing), blue (outward), black (others). **C**, Graphical interpretation of the data, showing the residues whose substitution changed the time course of open-channel desensitization. **D**, For WT and selected mutants the time constant of open-channel desensitization is plotted at different stimulation pH (n=3-21). The inset shows representative current traces of N416C-MTSET at different stimulation pH. **E**, Structural alignment of WT ASIC1 of the open structure 4FZ1 (green) and the desensitized structure (blue). N416 is

shown in orange **F**, Situation around N416 in the MD simulation of WT. **G**, Situation around R416 in the MD simulation of the N416R mutant. In all structural images the numbering of residues is according to human ASIC1a.

Fig. 4. Appearance of a sustained current in palm mutants. A, Representative current traces of mutants Q278C and L415C before (top) and after MTSET exposure (1 mM, 5 min; bottom). **B**, The sustained current fraction (I_{sust}/I_{peak}) measured at pH5 is plotted for Cys mutants before (open bars) and after exposure to MTSET (filled bars), n=3-15. *, different from WT ($p<0.05$ ANOVA, Dunnett's post test). Mutants are indicated in the color of their orientation, red (inward facing), blue (outward), black (others). For L415C the small peak-like deflection was not considered as peak for calculating the ratio. The mutant Y417C displayed a small sustained current. Exposure to MTSET decreased the peak current amplitude by 17 ± 2 - fold but did not affect the I_{sust} (n=9), resulting in the high I_{sust}/I_{peak} ratio observed.
C, Graphical interpretation of the data. Residues whose substitution resulted in $I_{sust} > 0.1$ at pH5 and was significantly different from WT I_{sust} are shown; orange, $I_{sust}/I_{peak} > 0.1$ in Cys mutant or Cys-MTSET; green, $I_{sust}/I_{peak} > 0.3$ in Cys mutant or Cys-MTSET. **D**, Role of side chain properties of desensitization mutants. The sustained current fraction is plotted for the mutation to Arg, and to Cys before and after modification by MTSET (positively charged), MTSES (negatively charged) and a non-charged hydrophobic reagent (DMBE-MTS), n=3-12. Data are from stimulation pH4.5, except for L415C-MTSET and L415R, average of I_{sust} obtained at pH4 and pH5.

Fig. 5. Molecular dynamics analysis of desensitization mutants. A, Radius of the solvent-accessible cavities and pores along the central vertical channel axis, calculated with the HOLE software (22). "Channel axis" refers to the position along the vertical axis as indicated in B. Calculations were made from MD simulations of WT and the indicated mutants obtained as average over 200 frames, and from the open crystal structure of Psalmotoxin-bound ASIC1 at pH7.25 (PDB number 4FZ1 (5)). **B**, Mapping of the solvent-accessible pathway, shown for the desensitized structure (PDB 2QTS). **C**, Schematic view of the channel seen from the bottom, showing three β strands per subunit and highlighting the orientation of residues L77 (turquoise), Q276 (orange) and L280 (green) in the desensitized WT structure. **D, G-I**, Detail views taken at the end of the MD simulations. Subunits are shown in different colors and the residues L77 in turquoise, Q276 in orange and L280 in green. Note that the views are from the inside of the central vestibule. **D**, View of WT, showing the positions and the environment of

L77, Q276 and L280. **E, F**, Structure alignment of WT (blue) and the mutant L280R (yellow) obtained at the end of the MD simulations. **E,** Side view (subunit A). **F**, View from bottom. The red arrows highlight the main differences between the mutant and WT. The letters in (F) indicate the subunits, with subunit A shifted outward. **G-I**, Detail view of the L280R mutant (**G**), the L77R mutant (**H**) and the Q276R mutant (**I**). In all structural images the numbering of residues is according to human ASIC1a.

Fig. 6. The mutation L415R induces strong conformational changes in the lower palm domain. A, Alignment of the closed and desensitized ASIC1 crystal structure. Green, open; Blue, desensitized; L415 is shown in orange. **B-D**, The structures correspond to conformations adopted at the end of the MD simulation, seen from the outside. The residue at position 415 is shown in orange. **B**, Environment of L415 in the WT. **C**, Environment of the R415 side chain in the L415R mutant, as observed in two of three subunits in the MD simulation. R415 interacts by hydrogen bonds with E254 of a neighboring subunit. **D**, Environment of R415 in the L415R mutant, as observed in one subunit. The R415 side chain points downwards, changing the conformation of the lower palm β sheet of the same subunit. **E**, pH dependence of I_{sust} of L415 substitutions, n=3-39; **F**, pH dependence of activation of L415 substitutions, n=4-39. In all structural images the numbering of residues is according to human ASIC1a.

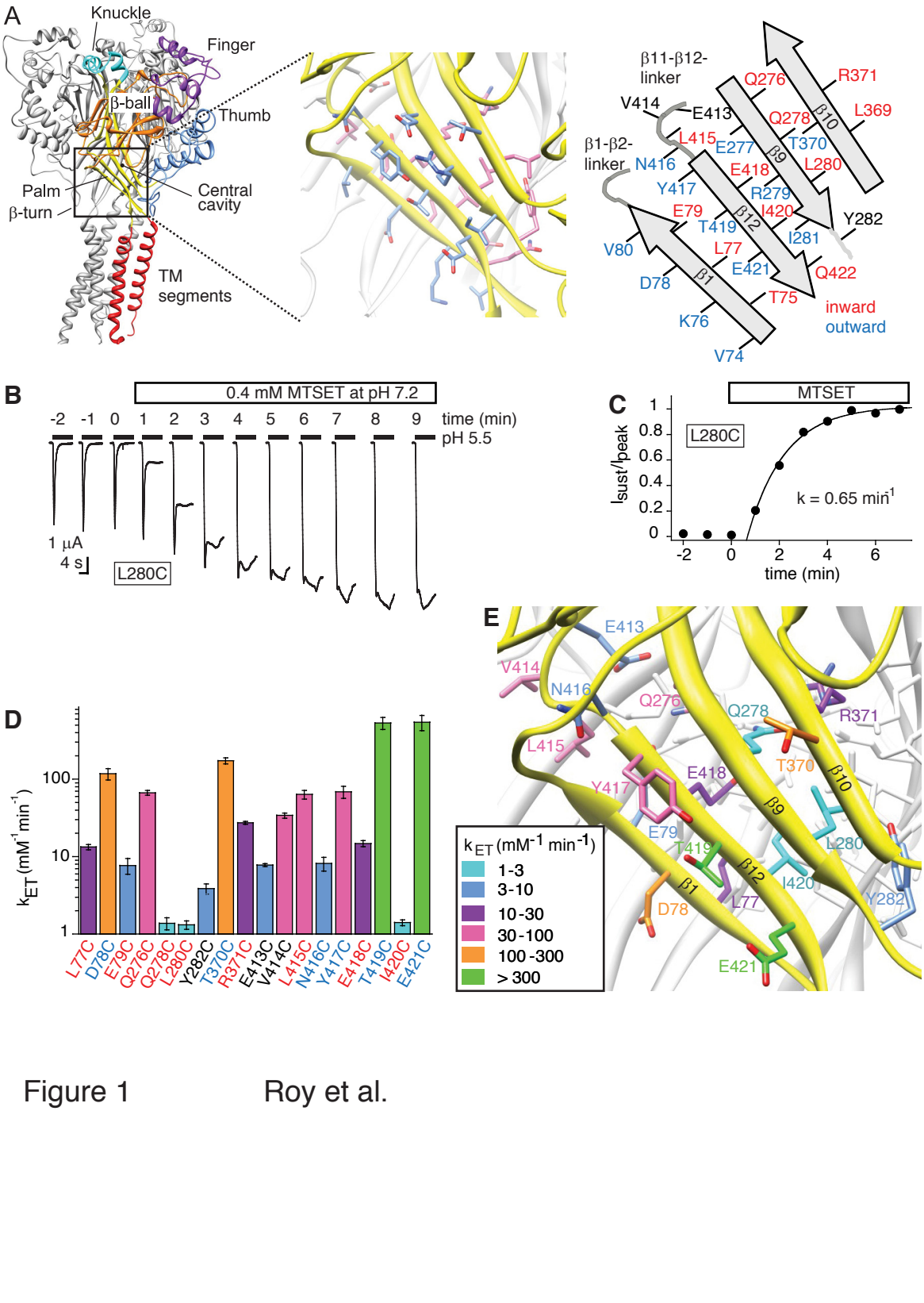

Figure 1 Roy et al.

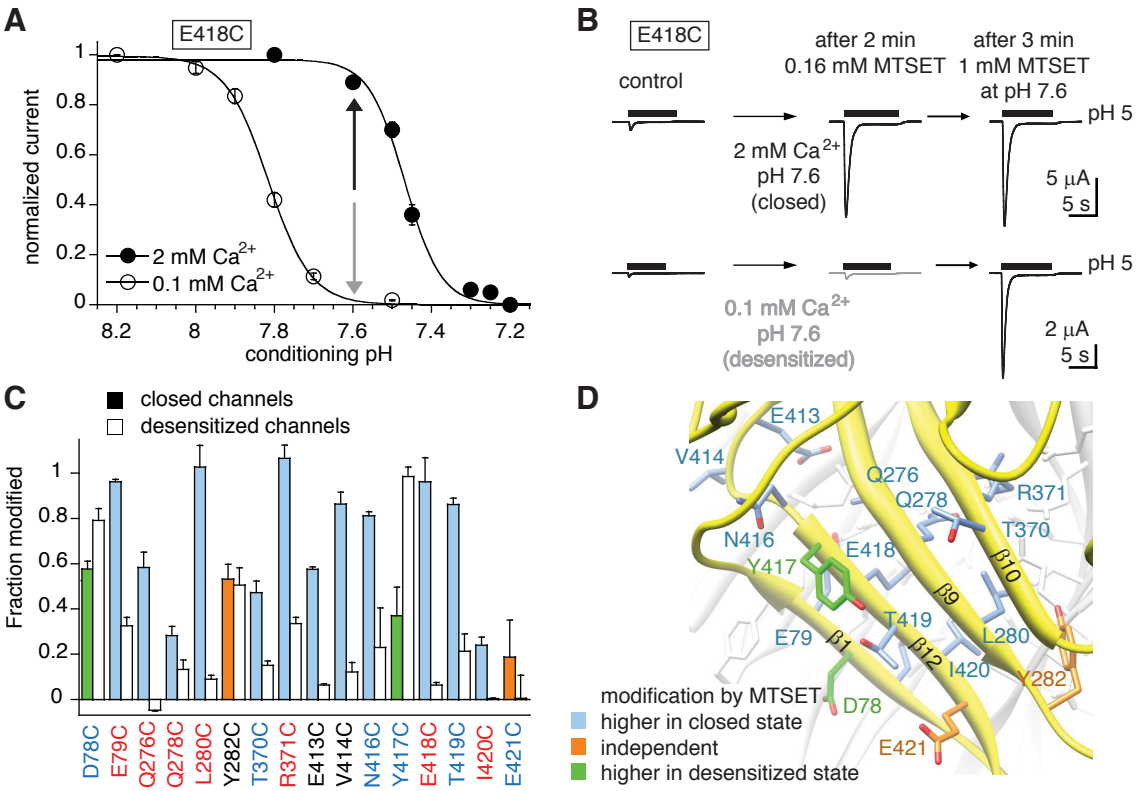

Figure 2 Roy et al.

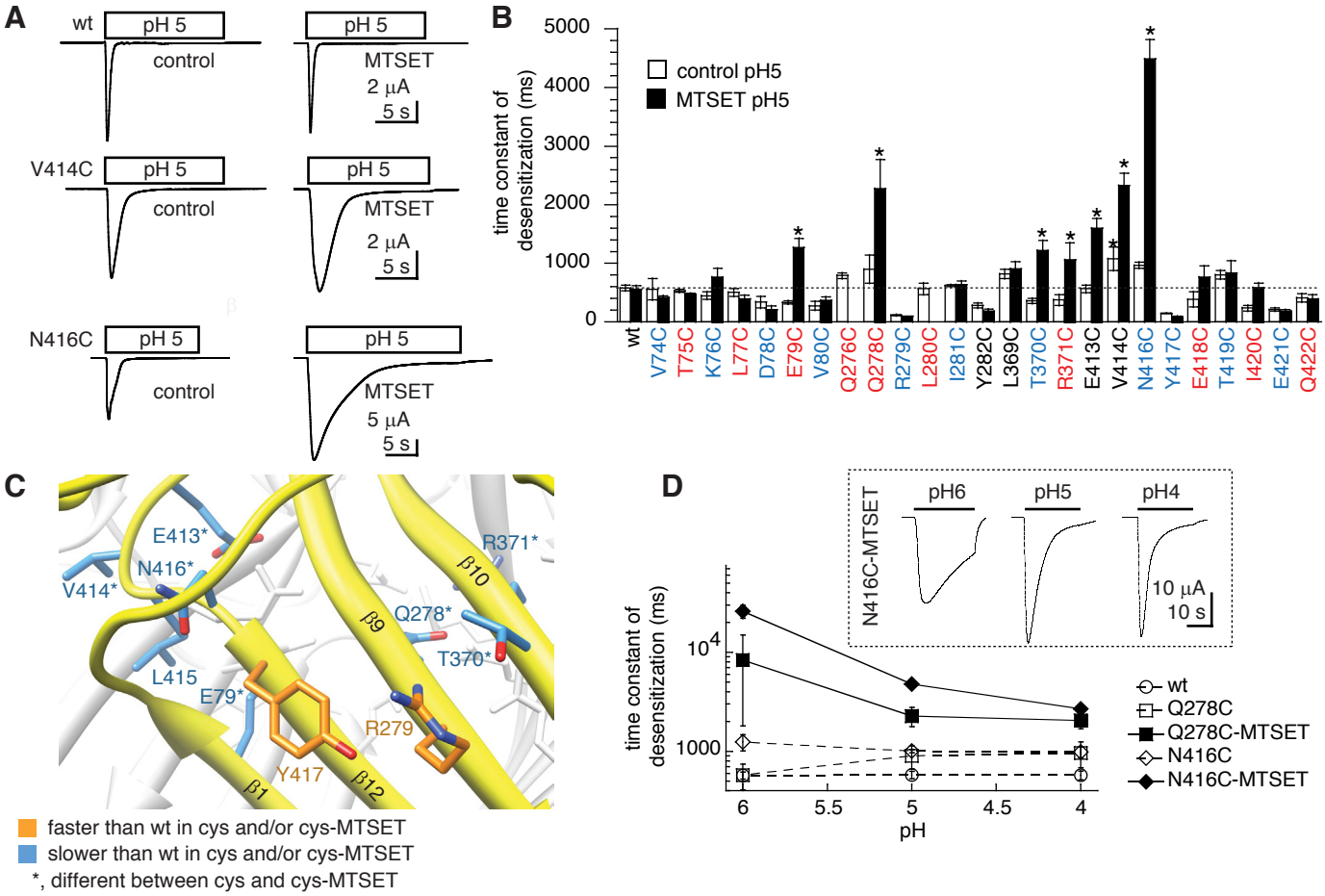

Figure 3 Roy et al.

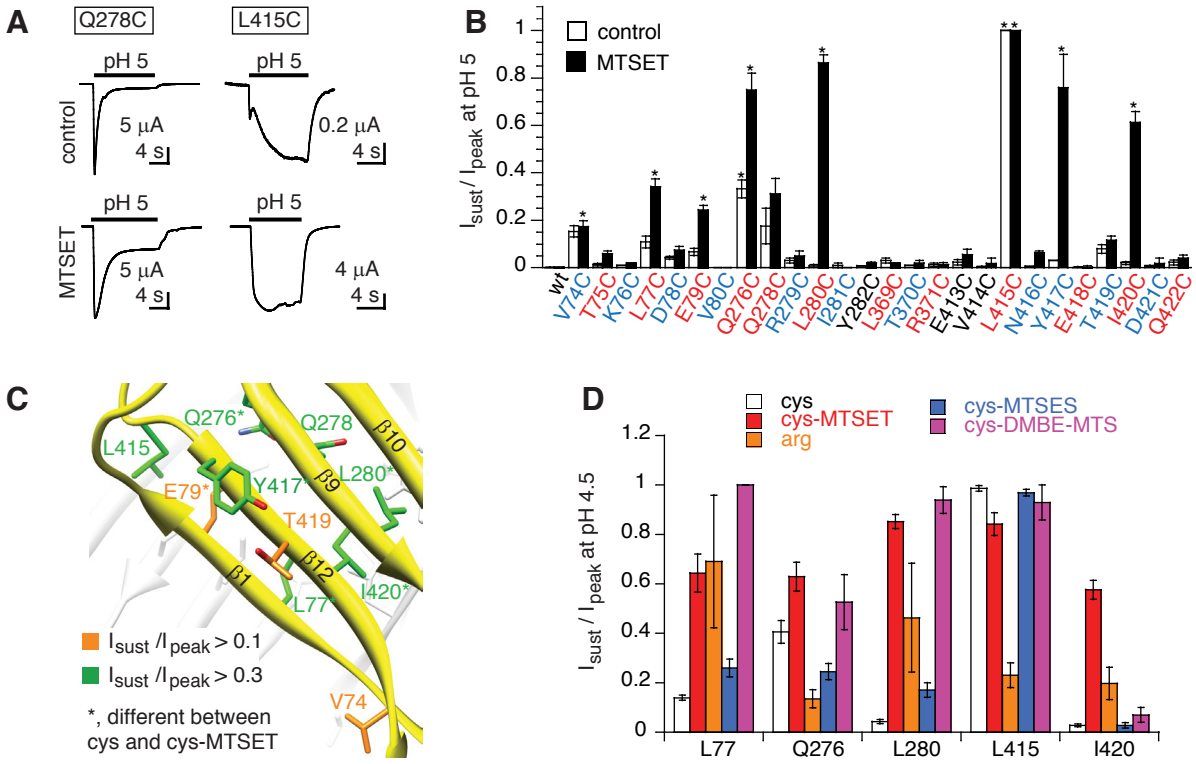

Figure 4 Roy et al.

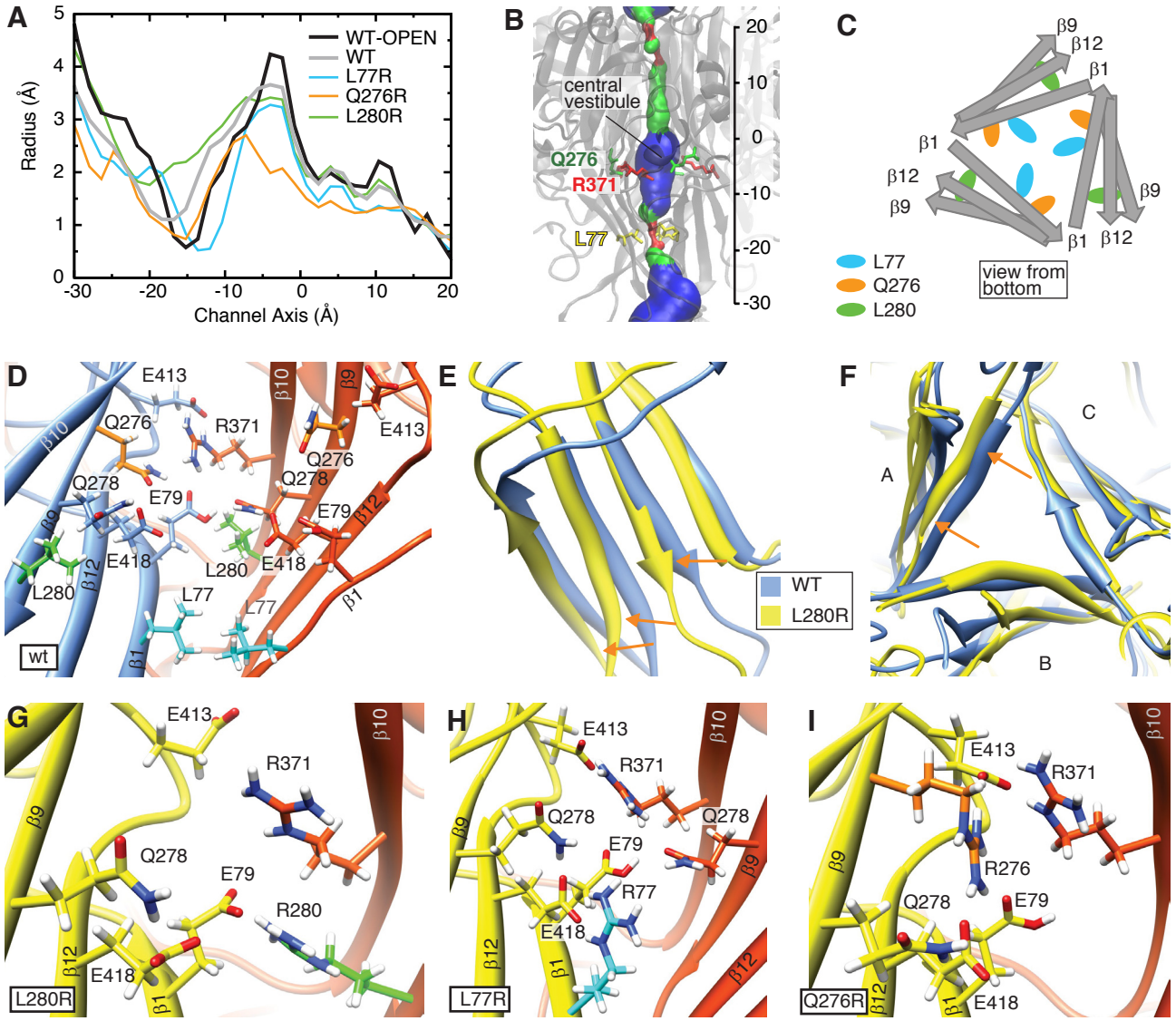

Figure 5 Roy et al.

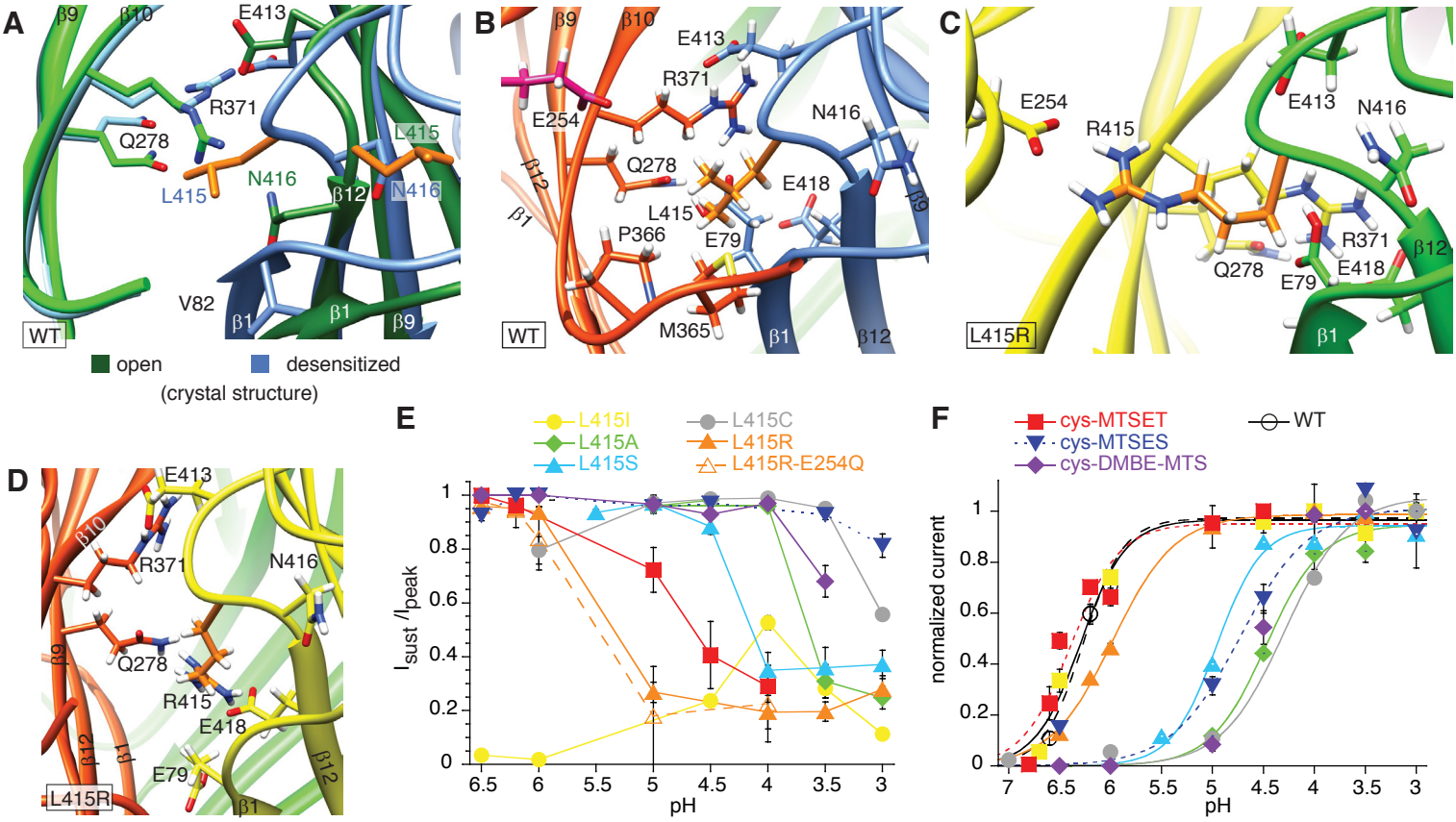

Figure 6 Roy et al.

Supplemental Table S1. Conditions for MTSET kinetics and state-dependent accessibility experiments

	MTSET kinetics to closed channels				state-dependent accessibility		
Mutant	conditioning pH	stimulation pH	observed change after MTSET	cause	pHDes50 at 2 mM Calcium	pHDes50 at 0.1 mM Calcium	incubation pH with MTSET
WT					7.19 ± 0.00	7.48 ± 0.00	
L77C	7.4	5	Isust				
D78C	7.4	6	I↑	pH50 shift	7.15 ± 0.01	7.50 ± 0.00	7.3
E79C	7.4	5.5	I↓		7.31 ± 0.01	7.61 ± 0.00	7.5
Q276C	7.2	5	Isust ↑		6.83 ± 0.00	7.04 ± 0.02	6.9
Q278C	7.2	6.7	I↑	pH50 shift	6.90 ± 0.02	7.17 ± 0.01	7.0
L280C	7.2	5.5	Isust, I↑		7.00 ± 0.00	7.23 ± 0.00	7.1
Y282C	7.4	5	I↓		7.09 ± 0.01	7.55 ± 0.01	7.4
T370C*	7.2	5	I↑	pHDes50 shift	7.26 ± 0.01	7.53 ± 0.00	7.4
R371C*	7.1	5.5	I↑	pHDes50 shift	7.19 ± 0.01	7.51 ± 0.00	7.3
E413C	7.2	6.2	I↓	pH50 shift	6.87 ± 0.01	7.13 ± 0.00	7.0
V414C	7.4	6.5	I↓	pH50 shift	7.13 ± 0.02	7.32 ± 0.01	7.3
L415C	7.4	5	I↑	pH50 shift			
N416C	7.2	6.5	I↓	pH50 shift	6.88 ± 0.01	7.22 ± 0.00	7.1
Y417C	7.4	5.5	I↓		7.47 ± 0.01	7.88 ± 0.06	7.6
E418C*	7.4	5	I↓	pHDes50 shift	7.47 ± 0.01	7.82 ± 0.00	7.6
T419C*	7.1	6	I↑	pHDes50 shift	7.18 ± 0.01	7.51 ± 0.00	7.4
I420C	7.4	5	Isust		7.09 ± 0.01	7.39 ± 0.00	7.2
E421C	7.4	5	I↓		7.17 ± 0.01	7.45 ± 0.00	7.3

The left part of the table describes the conditions for the MTSET kinetics experiments of Fig. 1 while the right part describes the conditions in the state-dependent accessibility experiments (Fig. 2). I ↑, current increase; I↓, current decrease; I_{sust}, sustained current; pH50, pH of half-maximal activation; pHDes50, pH of half-maximal steady-state desensitization; incubation pH with MTSET, pH at which the 2-min incubation with MTSET was carried out (Fig. 2), n=4-63. *, For the mutants T70C, R371C, E418C and T419C MTSET was applied to channels that were partially desensitized in the initial measurements of the time course of modification. Modification induced a right shift in the steady-state desensitization curve and thereby increased the current. The rate constants determined were 17.8 ± 2.8 mM^{-1} min^{-1} (T370C), 1.2 ± 0.0 mM^{-1} min^{-1} (R371C), 2.3 ± 0.4 mM^{-1} min^{-1} (E418C) and 42.6 ± 3.6 mM^{-1} min^{-1} (T419C). To provide MTSET modification rates to closed channels for these four mutants, protocols as described in Fig. 2B were used and MTSET was applied for 2 min at a pH at which the mutants were in the closed state. The concentration of MTSET was chosen to produce a 55-75% modification. From the fractional modification and the assumption of single exponential modification kinetics the modification rate was calculated. This modification rate is presented for these four mutants in Fig. 1D.

Supplementary Table S2. pH dependence of mutants

Mutant	pH50 Cys	pH50 Cys-MTSET	pHDes50 Cys	pHDes50 Cys-MTSET
WT	6.26 ± 0.01	6.25 ± 0.03	7.19 ± 0.00	7.16 ± 0.01
V74C	6.15 ± 0.05	6.22 ± 0.04	7.33 ± 0.02 *	7.32 ± 0.00 *
T75C	5.86 ± 0.03 *	5.84 ± 0.03 *	7.16 ± 0.01	7.16 ± 0.01
K76C	6.22 ± 0.03	6.52 ± 0.03 *	7.21 ± 0.01	7.14 ± 0.01
L77C	6.18 ± 0.03	6.12 ± 0.05 *	7.16 ± 0.01	7.31 ± 0.01 *
D78C	6.03 ± 0.02 *	5.95 ± 0.04 *	7.15 ± 0.01 *	7.18 ± 0.02
E79C	6.12 ± 0.03 *	6.22 ± 0.03	7.31 ± 0.01 *	6.71 ± 0.00 *
V80C	6.18 ± 0.04	6.12 ± 0.06	7.14 ± 0.00 *	7.09 ± 0.01 *
Q276C	6.26 ± 0.05	6.12 ± 0.03 *	6.83 ± 0.00 *	6.58 ± 0.01 *
Q278C	6.37 ± 0.08	6.44 ± 0.04 *	6.90 ± 0.02 *	6.82 ± 0.01 *
R279C	5.71 ± 0.08 *	5.54 ± 0.10 *	7.51 ± 0.01 *	7.48 ± 0.02 *
L280C	6.18 ± 0.02	6.46 ± 0.03 *	7.00 ± 0.00 *	6.86 ± 0.16 *
I281C	6.29 ± 0.03	6.13 ± 0.02 *	7.09 ± 0.01 *	7.10 ± 0.00 *
Y282C	6.11 ± 0.07	6.02 ± 0.07 *	7.09 ± 0.01 *	7.09 ± 0.01 *
L369C	6.41 ± 0.04	6.24 ± 0.04	7.10 ± 0.01 *	6.98 ± 0.00 *
T370C	6.20 ± 0.02	6.21 ± 0.05	7.26 ± 0.01 *	7.09 ± 0.00 *
R371C	6.21 ± 0.05	6.25 ± 0.03	7.19 ± 0.01	7.04 ± 0.01 *
V414C	6.36 ± 0.04	6.25 ± 0.02	7.13 ± 0.02 *	6.77 ± 0.03 *
L415C	4.13 ± 0.03 *	6.14 ± 0.06	N.D.	6.65 ± 0.09 *
N416C	6.23 ± 0.06	6.05 ± 0.02 *	6.88 ± 0.01 *	6.58 ± 0.07 *
Y417C	5.84 ± 0.08 *	5.83 ± 0.25 *	7.47 ± 0.01 *	7.53 ± 0.04 *
T419C	6.24 ± 0.02	6.30 ± 0.01	7.18 ± 0.01	7.08 ± 0.01 *
I420C	5.99 ± 0.02 *	6.12 ± 0.02 *	7.09 ± 0.01 *	6.56 ± 0.06 *
E421C	6.27 ± 0.03	6.19 ± 0.03	7.17 ± 0.01	7.16 ± 0.02
Q422C	6.07 ± 0.05 *	6.08 ± 0.04	7.24 ± 0.01 *	7.22 ± 0.02

The pH of half-maximal activation pH50, as well as the pH of half-maximal steady-state desensitization pHDes50 are plotted for the mutants indicated, before (Cys) and after exposure to MTSET (Cys-MTSET, n=3-63). *, different from WT, $p<0.05$; N.D., not determined..

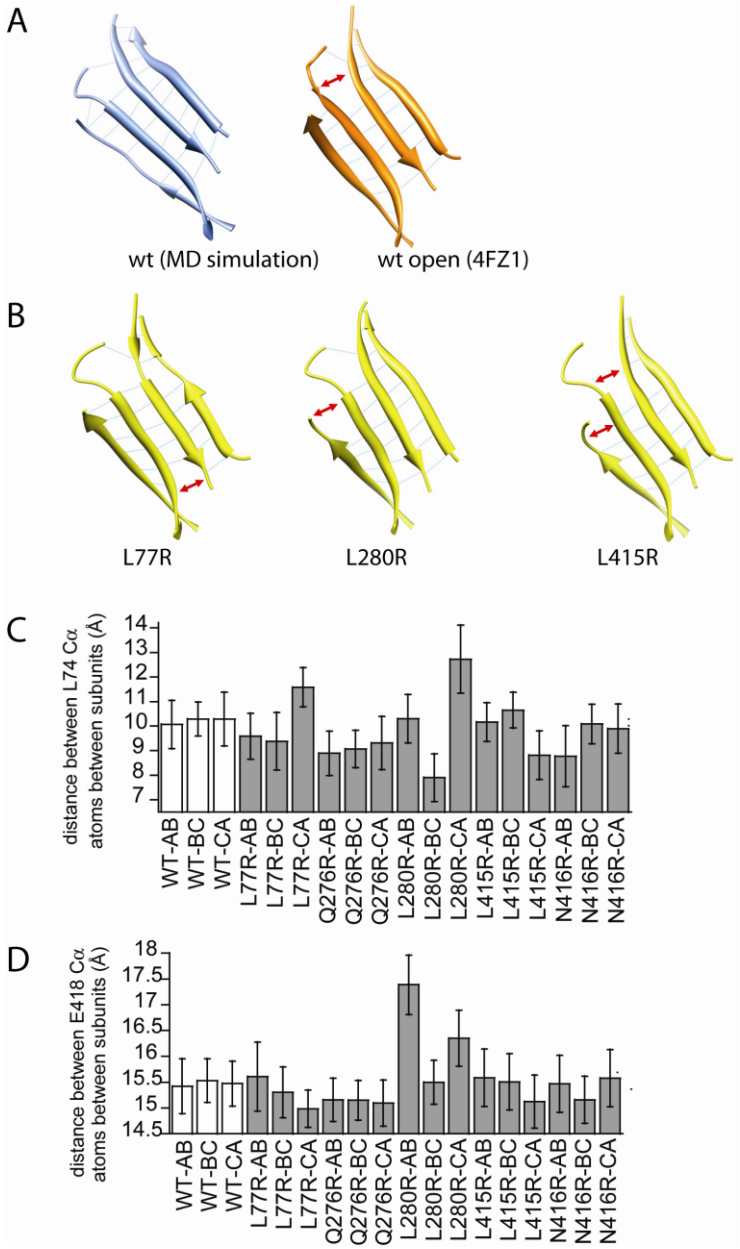

Supplementary Figure S1. Conservation of β sheet structure and intersubunit distance changes in mutants analyzed by MD simulations. A, illustration of the palm β sheet structure with indication of hydrogen bonds of the WT structure in the MD simulation (left) and the WT open structure (PDB 4FZ1) (right). Differences are highlighted with a red arrow. **B**, Illustration of the palm β sheet with indication of differences to WT in L77R, L280R and one of the three subunits of L415R. Differences to WT are indicated with red arrows. **C**, mean values of the intersubunit distance between L74 Cα atoms, measured in simulations with WT and different mutants. **D**, intersubunit distance between E418 Cα atoms, measured in simulations with WT and different mutants. For C and D, the mean values over the complete duration of the simulation are shown, between subunits A and B, B and C or C and A, as indicated.

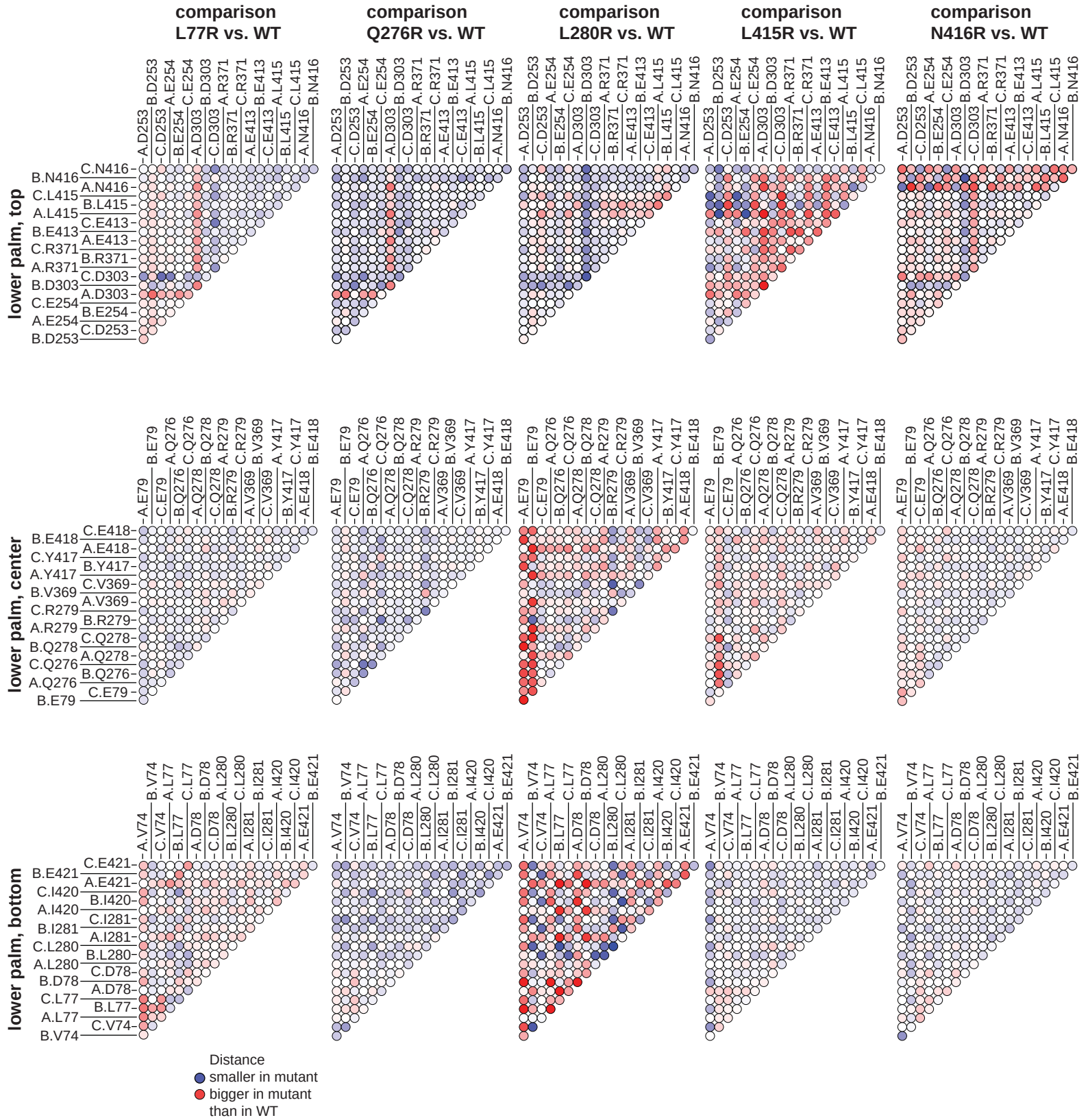

Supplementary Figure S2. Distance comparison with contact maps in mutants L77R, Q276R, L280R, L415R and N416R. Distances between the center of mass of the indicated residues were calculated for WT and the mutants L77R, Q276R and L280R, as an average from different time points of the MD simulation. These distances in each of the mutants were then compared to the distances in WT. Distances that were bigger in the mutant are indicated in red in the contact map, distances that were smaller in the mutant are indicated in blue. The intensity of the color is proportional to the difference in distance. Distances were measured in three different layers of the lower palm domain, separated into “bottom”, “center” and “top”. The amino acid residues according to the human ASIC1a WT are indicated; A, B and C stand for the three subunits.